FULL PAPER

Transparent, Flexible Films Based on Layered Double Hydroxide/Cellulose Acetate with Excellent Oxygen Barrier Property

Yibo Dou, Simin Xu, Xiaoxi Liu, Jingbin Han, Hong Yan, Min Wei, David G. Evans, and Xue Duan*

Transparent and flexible multilayer films are fabricated based on the alternating assembly of cellulose acetate (CA) and layered double hydroxide (LDH) nanoplatelets followed by thermal annealing treatment. The films exhibit tremendously enhanced oxygen barrier properties. The oxygen transmission rate (OTR) of the resulting $(CA/LDH)_n$ multilayer films can be tuned by changing the aspect ratio of high-crystalline LDH nanoplatelets from 20 to 560. The $(CA/LDH)_{20}$ film displays excellent oxygen-barrier behavior with an OTR equal to or below the detection limit of commercial instrumentation (<0.005 cm^3 m^{-2} day^{-1}), much superior to the previously reported inorganic flake-filled barrier film. Molecular dynamics simulations reveal that a hydrogen bonding network occurs at the interface of highly oriented LDH nanoplatelets and CA molecules, accounting for the suppression of oxygen transportation and the resulting largely improved barrier behavior. In addition, the durability of $(CA/LDH)_n$ films against humidity, temperature, and light irradiation is successfully demonstrated, which would guarantee their practical application. Therefore, this work provides a facile and cost-effective strategy for the fabrication of an LDH-based oxygen barrier material, which could potentially be used in flexible displays and drug and food packaging.

1. Introduction

Recently, flexible and transparent polymeric packaging materials have attracted considerable attention in the fields of electronics,[1,2] druggery and food preservation.[3] The effectiveness of polymer packaging materials in preventing product degradation is directly dependent upon their impermeability to degradative gases (e.g., O_2). Polymers are normally lightweight, inexpensive and easily processable, but their performance is often limited by high gas permeability.[4,5] Interestingly, inorganic flake-filled polymers have been demonstrated with enhanced barrier behavior, since the incorporated inorganic flakes induce permeating molecule to undergo an extensive diffusion path. This increased diffusion length, generally referred to as a tortuous pathway, is the key factor to high barrier systems.[6–8] Although the addition of inorganic nanoflakes into polymers boosts up the gas barrier property relative to the pristine polymer, currently reported nanoplatelets with limited aspect ratios and nonuniform particle size restrict a further improvement.[9–11] Moreover, the random alignment and weak bonding between inorganic species and polymer matrix result in the aggregation of inorganic component as well as phase separation, which gives rise to the decrease in barrier behavior.[12–14] Therefore, it is highly essential to explore new materials or approaches to obtain superior barrier films for packaging applications.

Layered double hydroxides (LDHs), whose structure can be generally expressed as $[M^{II}_{1-x}M^{III}_{x}(OH)_2](A^{n-})_{x/n}\cdot mH_2O$ (M^{II} and M^{III} are divalent and trivalent metals respectively, A^{n-} is interlayered anion), are one type of important layered materials with 2D-organized structure.[15–18] Recently, LDHs-based organic-inorganic functional materials have been widely explored in photoluminescence, optical devices, electrochemical sensors and pharmaceutical field.[19–22] The incorporation of LDH additives into polymers significantly enhances the mechanical, optical and thermal properties of polymer systems. This gives us impetus to take the challenge of fabricating oxygen barrier films based on LDH nanoplatelets/polymer. The assembly of LDH nanoplatelets within a polymer matrix for the preparation of oxygen barrier materials would possess the following advantages: firstly, LDH nanoplatelets with tunable aspect ratios is an ideal filling material for the enhancement of barrier property; secondly, the well-organized 2D structure imparts a high orientation of LDH nanoplatelets, which is expected to prolong the diffusion length of gas molecules and thus largely improve the impermeability of the film materials.

In this work, we report the $(CA/LDH)_n$ multilayer films with tunable oxygen barrier behavior fabricated by spin-coating of cellulose acetate (CA) and LDH nanoplatelets alternately, followed by thermal annealing treatment (**Scheme 1**). The oxygen transmission rate (OTR) of $(CA/LDH)_n$ multilayer films can be tailored by tuning the aspect ratio (α) of high-crystalline LDH nanoplatelets from 20 to 560. The resulting $(CA/LDH)_{20}$

Y. Dou, S. Xu, X. Liu, Dr. J. Han, Dr. H. Yan,
Prof. M. Wei, Prof. D. G. Evans, Prof. X. Duan
State Key Laboratory of Chemical Resource Engineering
Beijing University of Chemical Technology
Box 98, Beijing, 100029, PR China
E-mail: weimin@mail.buct.edu.cn

DOI: 10.1002/adfm.201301775

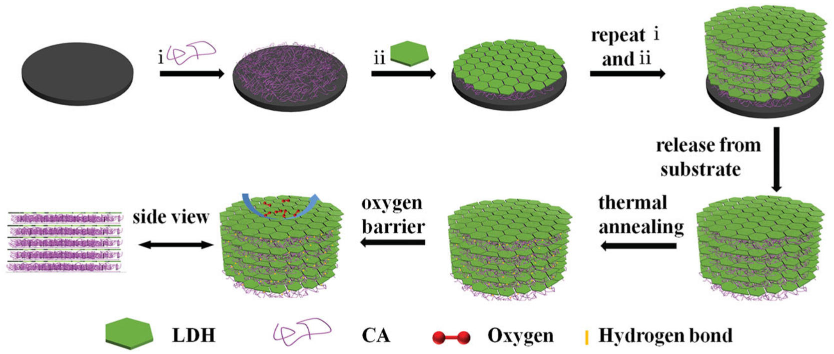

Scheme 1. Schematic representation for the fabrication of (CA/LDH)$_n$ films.

film exhibits excellent oxygen barrier property with OTR equal to or below the detection limit of commercial instrumentation (<0.005 cm^3 m^{-2} day^{-1}), superior to the previously reported inorganic flake-filled barrier films. This is attributed to the extremely large α of LDH nanoplatelets; furthermore, the formation of strong hydrogen bonding network in this highly-arrayed brick-and-mortar structure also contribute to the improvement of barrier property. In addition, molecular dynamics (MD) simulations reveal the oxygen diffusion coefficient decreases with the increase of aspect ratio of LDH flake, accounting for the largely-improved oxygen barrier behavior.

2. Results and Discussion

The MgAl-LDH nanoplatelets with various aspect ratio (α) were prepared by the hydrothermal method reported previously,[23,24] whose X-ray diffraction (XRD) pattern and Fourier transform infrared (FT-IR) spectrum (Figure S1 and S2) indicate a well-defined LDH with high crystallinity. The scanning electron microscope (SEM) images (**Figure 1**A and S3) reveal that MgAl-LDH platelets were obtained with lateral size of ~1.05, ~1.82, ~2.15, and ~3.42 µm. Employing an elemental mapping technique in transmission electron microscope (TEM), spatial elemental profiles of the platelet and a homogeneous distribution of Mg, Al and O atom are visualized in Figure 1B. In addition, the α values determined by atomic force microscope (AFM) images (Figure 1C and S4) are ~20, ~54, ~212, and ~560. Subsequently, the MgAl-LDH nanoplatelets were used as buliding blocks to fabricate (CA/LDH)$_n$ films by the spin-coating technique. UV–vis absorption spectra of the resulting (CA/LDH)$_n$ films (**Figure 2**A) show the characteristic absorption intensity of CA at 200 nm increases linearly with the increase of bilayer number n (**Figure 3**A, inset). Moreover, Figure 3B illustrates the dependence of the thickness of (CA/LDH)$_n$ films on the value of n. The approximately linear increase (from 4.4 um for 4 bilayers to 23.2 um for 20 bilayers) demonstrates a stepwise and regular film growth procedure.

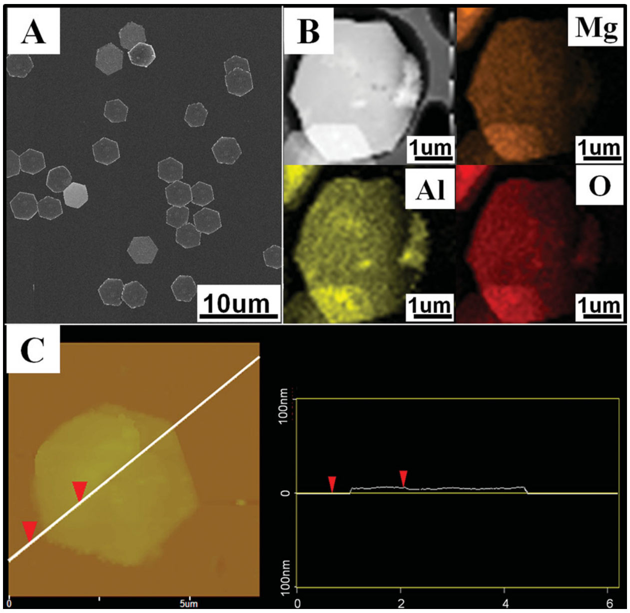

Figure 1. (A) SEM image, (B) TEM image and corresponding elemental maps of Mg, Al, and O, respectively, and (C) AFM image of MgAl-LDH flake.

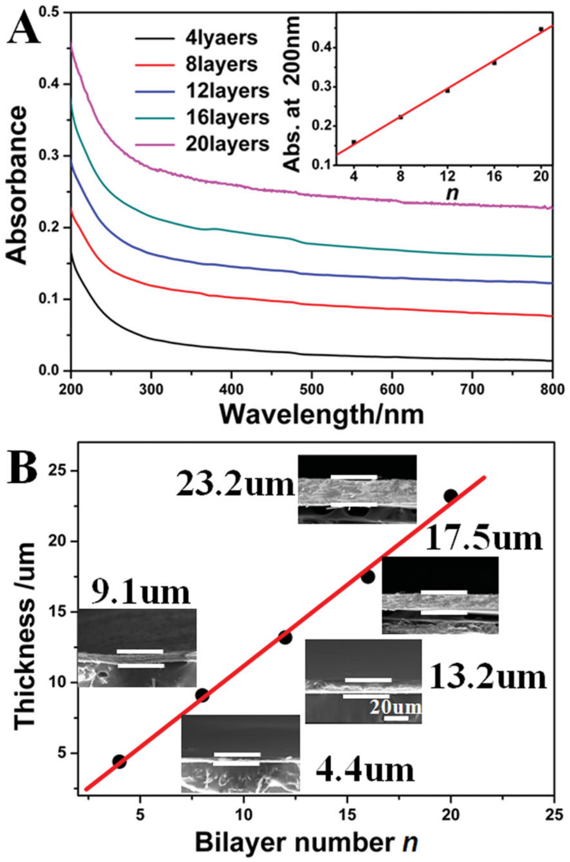

Figure 2. (A) UV–vis absorption spectra of the (CA/LDH)$_n$ (n = 4–20) films on quartz glass substrates (inset: the linear relationship between absorbance at 200 nm and bilayer number n). (B) Thickness of the (CA/LDH)$_n$ films as a function of bilayer number n (insets: the side-view SEM images. Scale bar = 20 um).

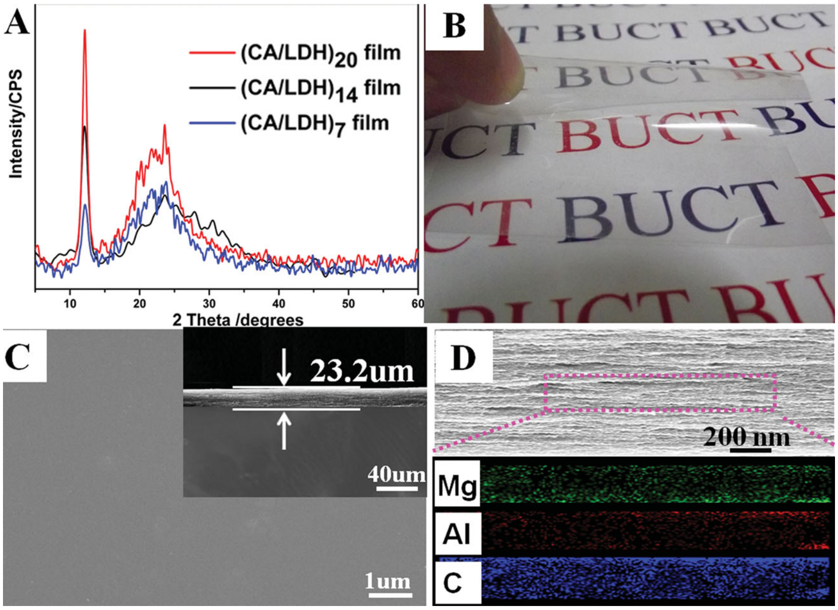

Figure 3. (A) XRD patterns of the $(CA/LDH)_n$ ($n = 7, 14, 20$) films. (B) A photograph, (C) top-view SEM image (inset: side-view SEM image) and (D) high magnification of side-view SEM image with corresponding EDX mapping analysis for the $(CA/LDH)_{20}$ film.

The XRD patterns (Figure 3A) for the obtained $(CA/LDH)_n$ ($n = 7, 14, 20$) films display a peak at 2θ 10.7° attributed to the (003) reflection of the LDH structure. The absence of any nonbasal reflections ($h, l \neq 0$) compared with LDH powdered sample (Figure S1) indicates a preferred orientation of LDH platelets with *ab* plane parallel to the substrate.[25,26] After release from the substrate, the $(CA/LDH)_{20}$ film exhibits high uniformity, flexibility and remarkable transparency with an average light transmittance of 90% across the visible-light spectrum (400–800 nm; Figure S5). The well-dispersed and oriented LDH nanoplatelets within CA matrix account for this high level of transparency (**Figure** 4B). The top-view and side-view SEM images of the $(CA/LDH)_{20}$ film (Figure 3C) exhibit a smooth and continuous surface with a thickness of 23.2 µm. Moreover, the high magnification of side-view (Figure 3D) shows that the uniform layered architecture consists of densely-packed LDH nanoplatelets with well *c*-orientation, consistent with the XRD result. In addition, the Mg, Al, and C are homogeneously distributed throughout the 2D-organized film by energy-dispersive X-ray (EDX) mapping analysis. AFM image shown in Figure S6 with the root-mean-square roughness of ~9.5 nm indicatevs a relatively smooth surface.

The interactions between CA and LDH nanoplatelets were investigated by means of XPS and FTIR technique. After combination of LDH and CA, the binding energy of Mg 2p

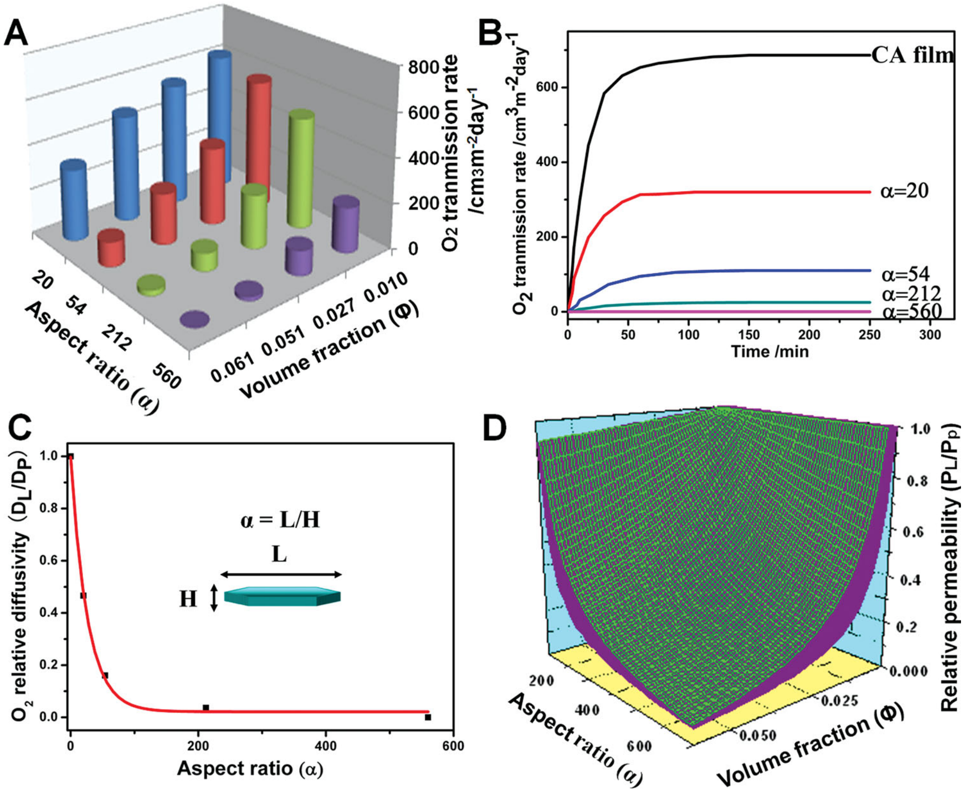

Figure 4. (A) The influences of α (20, 54, 212 and 560) and Φ_L (1.00%, 2.70%, 5.10%, and 6.10%) of LDH nanoplatelets on the OTR of $(CA/LDH)_{20}$ films. (B) The OTR curves for pristine CA film and $(CA/LDH)_{20}$ films ($\Phi_L = 6.10\%$) fabricated by LDH nanoplatelets with various α. (C) The relative diffusivity of $(CA/LDH)_{20}$ films as a function of α. (D) The comparison of LDH barrier mode (purple) with the Cussler mode (green).

Table 1. The oxygen barrier parameters for the pristine CA film and $(CA/LDH)_{20}$ films with various aspect ratios of LDH nanoplatelets (20, 54, 212 and 560, respectively).

Aspect ratio (α)	Film Thickness (d) [μm]	Oxygen transmission rates (OTRs) [$cm^3\ m^{-2}\ day^{-1}$]	Permeability (P) [$cm^3\ cm\ cm^{-2}\ s^{-1}\ mmHg^{-1}$] ($10^{-7}$)	Diffusivity (D) [$cm^2\ s^{-1}$] (10^{-5})	Solubility (S) [cm^3(STP) $cm^{-3}\ atm^{-1}$]
CA film	23.10	686.39	1.747	9.26	1.437
20	22.97	320.06	0.824	3.52	0.890
54	22.55	110.14	0.281	1.58	0.675
212	23.31	25.03	0.064	0.81	0.303
560	23.05	<0.005	—	—	—

(49.9 eV) and Al 2p (74.2 eV) in the MgAl-LDH shifts to 50.7 and 74.8 eV, respectively. Concomitantly, a decreased binding energy of C 1s (C–O–H in CA) from 284.4 eV to 283.7 eV is observed (Figure S7). The binding energy shift is indicative of an increased oxidation state of Mg and Al in MgAl-LDH and a decreased electron density of C in CA polymer, possibly resulting from the formation of hydrogen bonding between LDH nanoplatelets and CA by thermal annealing treatment.[27] In addition, a strong suppression of the lattice vibration of LDH at 678 cm^{-1} as well as the appearance of hydroxyl vibration in 800–1000 cm^{-1} were observed from FTIR spectra (Figure S8), further indicating the presence of hydrogen bonding in this clay-polymer composite material.[28,29]

The oxygen transmission rate (OTR) for pristine CA film and $(CA/LDH)_{20}$ films fabricated by LDH nanoplatelets with various aspect ratio α (20, 54, 212 and 560) and volume fraction (Φ_L: 1.00%, 2.70%, 5.10% and 6.10%) were investigated. Figure 4A reveals that the OTR of $(CA/LDH)_{20}$ films decreases dramatically by increasing either α or Φ_L. The OTR curves for pristine CA film and $(CA/LDH)_{20}$ films ($\Phi_L = 6.10\%$) fabricated by LDH nanoplatelets with various α are presented in Figure 4B, and the corresponding values of oxygen barrier parameters are summarized in **Table 1**. In contrast to the pristine CA film with OTR of 686.39 $cm^3\ m^{-2}\ day^{-1}$, the OTR of these $(CA/LDH)_{20}$ films decreases from 320.06 $cm^3\ m^{-2}\ day^{-1}$ to as low as less than the detection limit of commercial instrumentation (<0.005 $cm^3\ m^{-2}\ day^{-1}$) with the increase of α from 20 to 560. The results indicate the assembly of LDH nanoplatelets with CA polymer leads to a pronounced suppression of OTR. Moreover, the correlation between relative diffusion coefficients (D_L/D_P) and α of LDH flakes can be fitted by the following exponential equation: $D_L/D_P = 0.021 + 0.975\ e^{(-\alpha/26.26)}$, $r^2 = 0.998$. The relative diffusion coefficient decreases sharply as α increases from 20 to 212, and then remains constant with further enhancement of α up to 560. The result demonstrates the impermeable LDH flakes with larger α can effectively reduce the diffusion coefficient of oxygen (Figure 4C). Furthermore, the equation 1 of LDH barrier model is depicted based on the relative oxygen permeability coefficient (P_L/P_P) as a function of α and Φ_L:

$$\frac{P_L}{P_P} = \frac{1-\phi_L}{1+\left(\frac{2}{5}\right)\frac{\alpha}{2}\phi_L} \tag{1}$$

Both the increase of α (20, 54, 212 and 560) and Φ_L (1.00%, 2.70%, 5.10% and 6.10%) lead to a pronounced decrease of relative permeability (P_L/P_p). It is striking to see that the permeability coefficient of $(CA/LDH)_{20}$ films was much lower than that of predicted by Cussler model (Figure 4D),[30,31] which demonstrates that the tortuosity-based model can not explain the high barrier property of this LDH-based film system. This is attributed to the formation of hydrogen bonding network between LDH and CA, which induces an increased residence time of oxygen molecule and the resulting low permeability. It should be noted that compared with previously reported barrier films,[12,14,32–35] the $(CA/LDH)_{20}$ film in this work displays excellent balanced oxygen barrier behavior: much lower relative oxygen permeability (P_L/P_P) accompanied with a less thickness of ~23.2 μm (**Figure 5**).

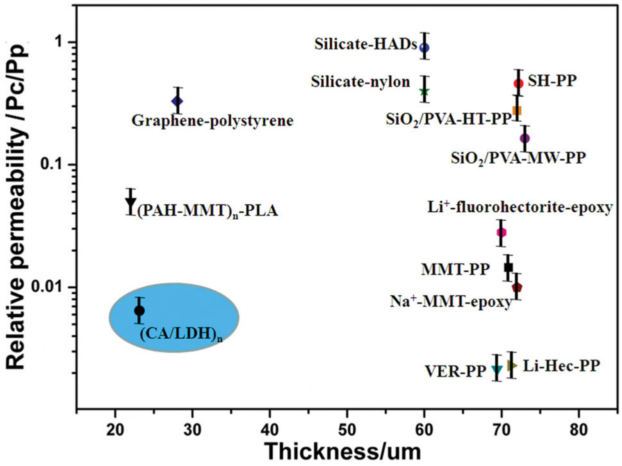

Figure 5. The relative oxygen transmission rate and thickness of the $(CA/LDH)_n$ film in this work, in comparison with previously reported barrier films: graphene-polystyrene film;[12] VER-PP, Li-Hec-PP, SH-PP, and MMT-PP film;[14] $(PAH\text{-}MMT)_n$-PLA film;[32] SiO_2/PVA-MW-PP and SiO_2/PVA-HT-PP film;[33] Li^+-fluorohectorite-epoxy and Na+-MMT-epoxy film;[34] silicate-HADs and silicate-nylon film.[35]

Taking into account potential applications of the $(CA/LDH)_n$ film, the pyrene solution with rather high oxygen sensitivity was applied to evaluate the oxygen barrier behavior.[36,37] The pyrene solution (0.01 M) stored in a bottle was capped with pristine CA film, CA-LDH film obtained by solvent evaporation method and $(CA/LDH)_{20}$ film, respectively, and the fluorescence emission spectra of the pyrene solution were recorded in situ. The correlation of fluorescence emission intensity at 378 nm (attributed to pyrene) as a function of storage time is shown in **Figure 6**. The fluorescence intensity of pyrene solution displays a consistent decrement capped by CA or CA-LDH

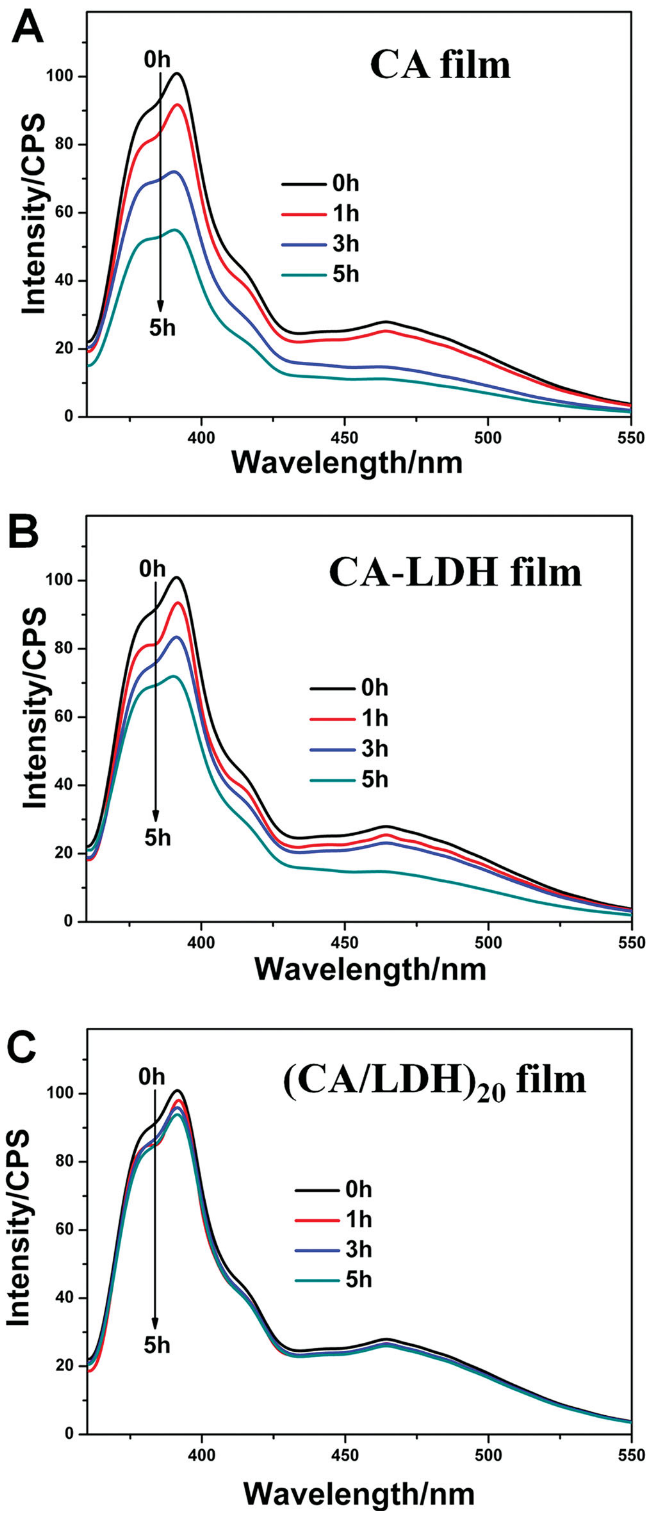

Figure 6. The fluorescence emission intensity of pyrene solution as a function of storage time capped by (A) pristine CA film, (B) CA-LDH film obtained by the solvent evaporation method and (C) (CA/LDH)20 film.

film; however, only tiny decrease in emission intensity was observed for the sample stored by $(CA/LDH)_{20}$ film, indicating its high oxygen barrier property. Moreover, the OTR behavior for pristine CA film, CA-LDH film and $(CA/LDH)_{20}$ film measured under various relative humidity and temperature is shown in Figure S9 and S10, respectively. The OTR of $(CA/LDH)_{20}$ film displays minimal variation compared with that of CA and CA-LDH film, demonstrating practical applications of the $(CA/LDH)_{20}$ barrier film against humidity and temperature. To test the lightfastness property, the $(CA/LDH)_{20}$ film was exposed under high-pressure Xe lamp for 6 months and the dependence of OTR on irradiation time is shown Figure S11. The results show that no obvious signal drift was observed for $(CA/LDH)_{20}$ film, demonstrating the lightfastness property of the composite film is enhanced significantly. This is attributed to the incorporation of LDH nanoplatelets which can reflect and absorb the UV light effectively.[38] Figure S12 displays repeated OTR measurements of 10 cycles for the barrier films, from which only the

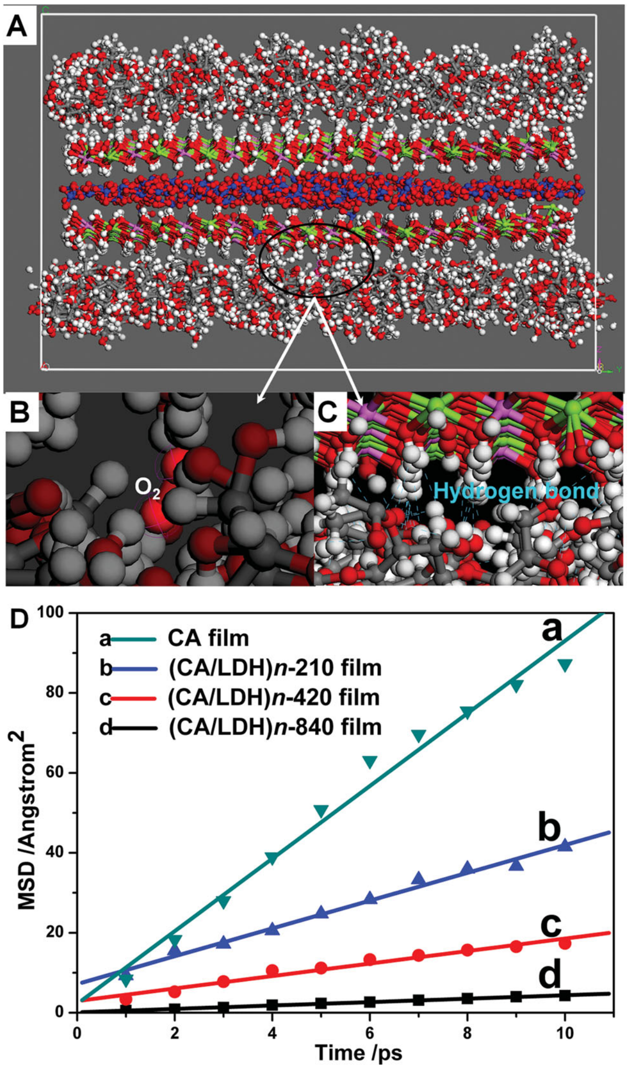

Figure 7. (A) The model geometry of $(CA/LDH)_n$-840 film after MD simulation and (B) the corresponding oxygen position after 60 ps. (C) The hydrogen bonding network in this system. (D) The mean square displacement (MSD) of oxygen as a function of time for CA film, $(CA/LDH)_n$-210 film, $(CA/LDH)_n$-420 film and $(CA/LDH)_n$-840 film.

$(CA/LDH)_{20}$ film keeps almost constant (RSD: 0.25%), in contrast to CA-LDH film (RSD: 1.03%) and CA film (RSD: 1.78%), indicating a long-term durability of the $(CA/LDH)_{20}$ film. In addition, no obvious change in the OTR value of $(CA/LDH)_{20}$ film was observed after bending 100 cycles, demonstraing its high flexibility and durability (Figure S13). The oriented (CA/LDH)20 film with brick wall structure also possesses a high thermal stability and satisfactory mechanical property, confirmed by TG and stress–strain curves (Figure S14 and S15). Therefore, the anti-humidity, heat-proof and lightfastness property as well as good durability favor (CA/LDH)n films serving as excellent barrier material with prospective applications in packaging materials.

Molecular dynamics (MD) simulations were further carried out to give a theoretical insight into the thermal motion of oxygen in this CA/LDH system. The MgAl-LDH flakes with the same thickness but various lateral sizes were incorporated with CA molecules by setting the number of metal atoms in one LDH platelet to be 210, 420, and 840. The three models are named $(CA/LDH)_n$-210 film, $(CA/LDH)_n$-420 film and $(CA/LDH)_n$-840 film, and the number of LDH flakes is 4, 2, and 1, respectively, to keep the volume fraction of LDH constant. For comparison, the pure CA film is also studied (the model geometries of CA film and $(CA/LDH)_n$ films are displayed in Figure S16, see the Supporting Information for details). After MD simulation, the geometries of CA and $(CA/LDH)_n$ models are shown in **Figure 7**A and Figure S17. Figure 7B shows the oxygen molecule moved from external surface into the $(CA/LDH)_n$-840 film after MD simulations of 60 ps, with the blocking of impermeable LDH nanoplatelets. In addition, the binding energy between CA and LDH was calculated to be as high as –4.472 eV per CA monomer based on first-principle calculations. The strong interaction indicates the existence of hydrogen bonding network (blue dashed line in Figure 7C) in this system, which was also confirmed the simulation results by using Materials Studio version 5.5 software package (Figure S18, see details in the Supporting Information). For each model, the plot of the mean squared displacement (MSD) of oxygen dependent on time is linearly fitted and displayed in Figure 7D. The corresponding diffusion coefficients are calculated to be 1.51×10^{-4}, 1.20×10^{-4}, 2.60×10^{-5} and 7.10×10^{-6} cm^2/s for CA film, $(CA/LDH)_n$-210 film, $(CA/LDH)_n$-420 film and $(CA/LDH)_n$-840 film, respectively. Obviously, the barrier behavior of $(CA/LDH)_n$ system towards oxygen is enhanced significantly along with the increase of aspect ratio of LDH flake, as a result of the decreased diffusion mobility of oxygen molecules.

3. Conclusions

$(CA/LDH)_n$ multilayer films have been fabricated via spin-coating CA and LDH nanoplatelets alternately followed by thermal annealing treatment, which exhibit tremendously enhanced gas barrier property. The $(CA/LDH)_n$ multilayer films display tailorable OTR by changing aspect ratio of high-crystalline LDH nanoplatelets from 20 to 560. In contrast to previously reported oxygen barrier materials, the highly-oriented LDH nanoplatelets as well as the hydrogen bonding network in this work induce a long diffusion length and strong resistance, thus suppressing the oxygen permeability. Furthermore, MD simulations reveal that the oxygen diffusion coefficient decreases with the increase of aspect ratio of LDH flake, accounting for the largely-improved oxygen barrier behavior. In addition, the durability of $(CA/LDH)_n$ films against humidity, temperature and light irradiation was successfully demonstrated, which would guarantee their practical applications. Therefore, the control over morphology of LDH fillings and organic-inorganic interactions demonstrated in this work offers a promising strategy for the development of gas barrier polymers, which can be potentially used in flexible electronics, artificial optical systems, food and drug packaging.

4. Experimental Section

Preparation of MgAl-LDH Nanoplatelets with Various Aspect Ratios: The MgAl-LDH nanoplatelets with particle size of ~1.05 and ~1.82 um were prepared as per a previously reported method:[24] Typically, 100 mL of solution A ($Mg(NO_3)_2{\cdot}6H_2O$: 0.20 M and $Al(NO_3)_3{\cdot}9H_2O$: 0.10 M) and 100 ml of solution B (urea: 1.00 M) were mixed together. The mixed solution was transferred into a Teflon-lined stainless steel autoclave, sealed, and hydrothermally treated at 110 °C for 10 h and 24 h, respectively. The resulting LDH slurry was obtained *via* centrifugation and washed with water and anhydrous ethanol for several times, and then dispersed in 400 ml of deionized water. The MgAl–LDH nanoplatelets with particle size of ~2.15 and ~3.42 um were synthesized by the procedure reported recently:[23] typically, $Mg(NO_3)_2{\cdot}6H_2O$ (0.20 mol), $Al(NO_3)_3{\cdot}9H_2O$ (0.10 mol), and hexamethylenetetramine (0.26 mol) were dissolved in an aqueous solution of 200 ml. The mixture was placed in an autoclave and heated at 140 °C for 9 h and 24 h, respectively. Subsequently, the resulting LDH slurry was obtained via centrifugation and washed with water and anhydrous ethanol for several times and then dispersed in 400 mL of deionized water.

Fabrication of $(CA/LDH)_n$ Multilayer Films: $(CA/LDH)_n$ multilayer films were fabricated by applying the spin-coating technique. The silicon wafer and quartz glass substrates were pre-cleaned with Piranha (H_2SO_4/H_2O_2, 3:1) solution for 30 min. The concentrations of CA polymer with 2.00% and LDH nanoplatelets with 0.05%, 0.15%, 0.25%, and 0.30% (wt%), respectively were used for the fabrication of films with various volume fraction of LDH. The CA solution (10 s per cycle, 4500 rpm) and LDH suspension (60 s per cycle, 2500 rpm) were spin-coated onto a silicon wafer or quartz glass substrate alternatively. The film was dried at ambient temperature in air for 10 min after each spin-coating process. Subsequently, a series of these operations for LDH and CA were repeated n times to obtain the $(CA/LDH)_n$ multilayer films. Finally, the $(CA/LDH)_n$ films was peeled off from the substrate and thermal annealing by the following process:[39,40] the film were placed in a sealed container purged with N_2 for 15 min, which was then slowly heated to 85 °C (approximately 1 h ramping time) and sustained for 2 h.

As a comparison sample, the CA-LDH film was obtained by the solvent evaporation method: LDH and CA solution were mixed together with stirring and contained in a glass vessel. Then the mixture was dried under nitrogen atmosphere at room temperature. Finally, the CA-LDH barrier film was peeled off from the bottom of the vessel.

Sample Characterization: X-ray diffraction (XRD) patterns were recorded by a Rigaku XRD-6000 diffractometer, using Cu Kα radiation (λ = 0.1542 nm) at 40 kV, 30 mA. The UV-vis absorption spectra were collected in the range 200–800 nm on a Shimadzu U-3000 spectrophotometer. The morphology was investigated using a scanning electron microscope (SEM; Zeiss SUPRA 55) with the accelerating voltage of 20 Kv, a FEI Cs-corrected Titan 80–300 high resolution transmission electron microscope (HRTEM) operated at 300 kV and a NanoScope IIIa atomic force microscope (AFM) from Veeco Instruments. The Fourier-transform infrared (FTIR) spectra were obtained using a Vector 22 (Bruker) spectrophotometer with 2 cm^{-1} resolution. Loading of LDH in the films were measured by inductively coupled plasma (ICP) emission spectroscopy (Shimadzu ICPS-7500). The fluorescence emission spectra were recorded in the range 360–550 nm, and both the excitation and emission slit were set to 3 nm. The measurements of the anti-light capability of the films were performed by exposing the films under a high-pressure Xe lamp (150 W, PerkinElmer Co.). Thermogravimetry and differential thermal analysis (TG–DTA) curves were obtained on a Beifen PCT-IA instrument in the temperature range 40–700 °C. The mechanical property of films was measured under tensile mode in a universal mechanical testing machine (Instron, FastTrack 8800 Servohydraulic Systems) with load speed of 0.5 mm/min. The specimen was obtained by cutting the film into 4 mm × 20 mm stripes. Oxygen transmission rates (OTRs) were collected using OX-TRAN model 8001E-net OTR tester (ILLINOIS Oxygen Permeation Analyzer) following Testing and Materials (ASTM) protocol GB/T 1038–2000. All permeability coefficient values were averaged from at least five separate films.

Supporting Information

Supporting Information is available from the Wiley Online Library or from the author.

Acknowledgements

This project was supported by the 973 Program (Grant No.: 2014CB932104), the National Natural Science Foundation of China (NSFC), the Collaboration Project from the Beijing Education Committee, the Fundamental Research Funds for the Central Universities (Grant No.: ZY1215). M. Wei particularly appreciates the financial aid from the China National Funds for Distinguished Young Scientists of the NSFC.

Received: May 23, 2013
Revised: July 1, 2013

---

[1] R. S. Kumar, M. Aucha, E. Ou, G. Ewald, C. S. Jin, *Thin Solid Films* **2002**, *417*, 120.

[2] P. E. Burrows, G. L. Graff, M. E. Gross, P. M. Martin, M. K. Shi, M. Hall, E. Mast, C. Bonham, W. Bennett, M. B. Sullivan, *Displays* **2001**, *22*, 65.

[3] a) R. S. Jagadish, B. Raj, M. R. Asha, *J. Appl. Polym. Sci.* **2009**, *113*, 3732; b) C. A. Phillips, *Int. J. Food Sci. Technol.* **1996**, *31*, 463.

[4] a) C. E. Goodyer, A. L. Bunge, *J. Membrane Sci.* **2009**, *329*, 209; b) C. S. Lu, Y. W. Mai, *Compos. Sci. Technol.* **2007**, *67*, 2895.

[5] a) H. R. Lusti, M. A. Osman, V. Mittal, *Macromol. Rapid Commun.* **2004**, *25*, 1145; b) D. A. Newsome, D. S. Sholl, *Nano Lett.* **2006**, *6*, 2150; c) W. S. Jang, I. Rawson, J. C. Grunlan, *Thin Solid Films* **2008**, *516*, 4819; d) A. A. Gusev, H. R. Lusti, *Adv. Mater.* **2001**, *13*, 164.

[6] a) G. L. Robertson, *Food Packaging: Principles and Practice*, CRC Press, Boca Raton, FL **2005**, pp.193–224; b) M. A. Priolo, D. Gamboa, K. M. Holder, J. C. Grunlan, *Nano Lett.* **2010**, *10*, 4970.

[7] a) G. Laufer, C. Kirkland, A. A. Cain, J. C. Grunlan, *Appl. Mater. Interfaces* **2012**, *4*, 1643; b) M. Alexandre, P. Dubois, *Mater. Sci. Eng. R* **2000**, *28*, 1.

[8] A. J. Svagan, A. Åkesson, M. Cárdenas, S. Bulut, J. C. Knudsen, J. Risbo, D. Plackett, *Biomacromolecules* **2012**, *13*, 397.

[9] a) M. A. Priolo, K. M. Holder, D. Gamboa, J. C. Grunlan, *Langmuir* **2011**, *27*, 12106; b) K. Kalaitzidou, H. Fukushima, L. T. Drzal, *Carbon* **2007**, *45*, 1446.

[10] M. A. Priolo, D. Gamboa, J. C. Grunlan, *Appl. Mater. Interfaces* **2010**, *2*, 312.

[11] a) J. L. Lutkenhaus, K. McEnnis, P. T. Hammond, *Macromolecules* **2008**, *41*, 6047; b) Y. H. Yang, L. Bolling, M. A. Priolo, J. C. Grunlan, *Adv. Mater.* **2013**, *25*, 503.

[12] O. C. Compton, S. Kim, C. Pierre, J. M. Torkelson, S. T. Nguyen, *Adv. Mater.* **2010**, *22*, 4759.

[13] T. Ebina, F. Mizukami, *Adv. Mater.* **2007**, *19*, 2450.

[14] M. W. Möller, T. Lunkenbein, H. Kalo, M. Schieder, D. A. Kunz, J. Breu, *Adv. Mater.* **2010**, *22*, 5245.

[15] a) Q. Wang, D. O'Hare, *Chem. Rev.* **2012**, *112*, 4124; b) G. R. Williams, D. O'Hare, *J. Mater. Chem.* **2006**, *16*, 3065; c) D. Yan, J. Lu, M. Wei, S. Qin, L. Chen, S. Zhang, D. G. Evans, X. Duan, *Adv. Funct. Mater.* **2011**, *21*, 2497; d) A. Illaik, C. Taviot-Guého, J. Lavis, S. Commereuc, V. Verney, F. Leroux, *Chem. Mater.* **2008**, *20*, 4854.

[16] a) J. Y. Uan, J. K. Lin, Y. S. Yung, *J. Mater. Chem.* **2010**, *20*, 761; b) A. M. Fogg, V. M. Green, H. G. Harvey, D. O'Hare, *Adv. Mater.* **1999**, *11*, 1466; c) X. Hou, R. J. Kirkpatrick, *Inorg. Chem.* **2001**, *40*, 6397; d) L. Hu, L. Wu, M. Liao, X. Hu, X. Fang, *Adv. Funct. Mater.* **2012**, *22*, 998.

[17] a) B. Monteiro, S. Gago, F. A. A. Paz, R. Bilsborrow, I. S. Gonçalves, M. Pillinger, *Inorg. Chem.* **2008**, *47*, 8674; b) F. Leroux, C. Taviot-Guého, *J. Mater. Chem.* **2005**, *15*, 3628; c) W. Shi, S. He, M. Wei, D. G. Evans, X. Duan, *Adv. Funct. Mater.* **2010**, *20*, 3856.

[18] a) M. C. Richardson, P. S. Braterman, *J. Phys. Chem. C* **2007**, *111*, 4209; b) J. W. Bocair, P. S. Braterman, *Chem. Mater.* **1999**, *11*, 298; c) G. R. Williams, T. G. Dunbar, A. J. Beer, A. M. Fogg, D. O'Hare, *J. Mater. Chem.* **2006**, *16*, 1231.

[19] a) S. Gago, T. Costa, J. S. de Melo, I. S. Gonçalves, M. Pillinger, *J. Mater. Chem.* **2008**, *18*, 894; b) S. Gago, M. Pillinger, R. A. S. Ferreira, L. D. Carlos, T. M. Santos, I. S. Gonçalves, *Chem. Mater.* **2005**, *17*, 5803; c) X. Hou, R. J. Kirkpatrick, *Chem. Mater.* **2002**, *14*, 1195; d) M. Zhao, Q. Zhang, X. Jia, J. Huang, Y. Zhang, F. Wei, *Adv. Funct. Mater.* **2010**, *20*, 677.

[20] a) J. L. Gunjakar, T. W. Kim, H. N. Kim, I. Y. Kim, S. J. Hwang, *J. Am. Chem. Soc.* **2011**, *133*, 14998; b) J. A. Kim, S. J. Hwang, J. H. Choy, *J. Nanosci. Nanotechnol.* **2008**, *8*, 5172; c) C. Chen, P. Gunawan, X. Lou, R. Xu, *Adv. Funct. Mater.* **2012**, *22*, 780.

[21] a) D. Yan, J. Lu, M. Wei, D. G. Evans, X. Duan, *J. Mater. Chem.* **2011**, *21*, 13128; b) A. Illaik, C. Taviot-Guého, J. Lavis, S. Commereuc, V. Verney, F. Leroux, *Chem. Mater.* **2008**, *20*, 4854; c) A. W. Myong, M. S. Song, T. W. Kim, I. Y. Kim, J. Y. Ju, Y. S. Lee, S. J. Kim, J. H. Choy, S. J. Hwang, *J. Mater. Chem.* **2011**, *21*, 4286; d) S. Gago, T. Costa, J. S. de Melo, I. S. Gonçalves, M. Pillinger, *J. Mater. Chem.* **2008**, *18*, 894.

[22] a) A. W. Myong, M. S. Song, T. W. Kim, I. Y. Kim, J. Y. Ju, Y. S. Lee, S. J. Kim, J. H. Choy, S. J. Hwang, *J. Mater. Chem.* **2011**, *21*, 4286; b) Q. Wang, H. Tay, D. Ng, L. Chen, Y. Liu, J. Chang, Z. Zhong, J. Luo, A. Borgna, *ChemSusChem* **2010**, *3*, 965; c) J. Y. Uan, J. K. Lin, Y. S. Yung, *J. Mater. Chem.* **2010**, *20*, 761.

[23] L. Li, R. Ma, Y. Ebina, N. Iyi, T. Sasaki, *Chem. Mater.* **2005**, *17*, 4386.

[24] a) Q. Tao, Y. Zhang, X. Zhang, P. Yuan, H. He, *J. Solid State Chem.* **2006**, *179*, 708; b) J. B. Han, J. Lu, M. Wei, Z. L. Wang, X. Duan, *Chem. Commun.* **2008**, *44*, 5188.

[25] J. Gursky, S. Blough, C. Luna, C. Gomez, A. Luevano, E. Gardner, *J. Am. Chem. Soc.* **2006**, *128*, 8376.

[26] a) M. Adachi-Pagano, C. Forano, J. P. Besse, *Chem. Commun.* **2000**, *36*, 91; b) E. Gardner, K. Huntoon, T. Pinnavaia, *Adv. Mater.* **2001**, *13*, 1263; c) M. Shao, M. Wei, D. G. Evans, X. Duan, *Chem. Commun.* **2011**, *47*, 3171.

[27] a) J. L. Stair, J. J. Harris, M. L. Bruening, *Chem. Mater.* **2001**, *13*, 2641; b) Z. Tang, N. A. Kotov, S. Magonov, B. Ozturk, *Nat. Mater.* **2003**, *2*, 413.

[28] P. F. Kiser, G. Wilson, D. A. Needham, *Nature* **1998**, *394*, 459.

[29] J. B. Han, Y. Dou, D. Yan, J. Ma, M. Wei, D. G. Evans, X. Duan, *Chem. Commun.* **2011**, *47*, 5274.

[30] a) L. E. Nielsen, *J. Macromol. Sci., Part A: Pure Appl. Chem.* **1967**, *1*, 929; b) R. K. Bharadwaj, *Macromolecules* **2001**, *34*, 9189; c) E. L. Cussler, S. E. Hughes, W. J. Ward III, R. Aris, *J. Membr. Sci.* **1988**, *38*, 161.

[31] a) C. E. Goodyer, A. L. Bunge, *J. Membr. Sci.* **2007**, *306*, 196; b) W. R. Falla, M. Mulski, E. L. Cussler, *J. Membr. Sci.* **1996**, *119*, 129.

[32] A. Laachachi, V. Ball, K. Apaydin, V. Toniazzo, D. Ruch, *Langmuir* **2011**, *27*, 13879.

[33] K. Kuraoka, A. Hashimoto, *J. Ceram. Soc. Jpn.* **2008**, *116*, 832.

[34] K. S. Triantafyllidis, P. C. LeBaron, I. Park, T. J. Pinnavaia, *Chem. Mater.* **2006**, *18*, 4393.

[35] G. M. Russo, G. P. Simon, L. Incarnato, *Macromolecules* **2006**, *39*, 3855.

[36] Y. Fujiwara, Y. Amao, *Sens. Actuat. B* **2003**, *89*, 187.

[37] B. J. Basu, K. S. Rajam, *Sens. Actuat. B* **2004**, *99*, 459.

[38] D. Yan, J. Lu, M. Wei, S. Li, D. G. Evans, X. Duan, *Phys. Chem. Chem. Phys.* **2012**, *14*, 85913.

[39] J. L. Stair, J. J. Harris, M. L. Bruening, *Chem. Mater.* **2001**, *13*, 2641.

[40] L. Mariniello, C. Giosafatto, P. Pierro, A. Sorrentino, R. Porta, *Biomacromolecules* **2010**, *11*, 2394.